

A Robust Real-Time Lane Detection Method with Fog-Enhanced Feature Fusion for Foggy Conditions

Ronghui Zhang^a, Yuhang Ma^a, Tengfei Li^a, Ziyu Lin^a, Yueying Wu^a, Junzhou Chen^{a,*}, Lin Zhang^b, Jia Hu^c, Tony Z. Qiu^d and Konghui Guo^e

^aGuangdong Provincial Key Laboratory of Intelligent Transportation System, School of Intelligent Systems Engineering, Sun Yat-sen University, Guangzhou, 510275, China

^bCollege of Automotive Studies, Tongji University, Shanghai, 201804, China

^cCollege of Transportation Engineering, Tongji University, Shanghai, 201804, China

^dDepartment of Civil and Environmental Engineering, University of Alberta, Edmonton, Alberta, Canada

^eState Key Laboratory of Automotive Chassis Integration and Bionics, Jilin University, Changchun, 130025, China

ARTICLE INFO

Keywords:

ADAS
Intelligent vehicle
Foggy lane detection dataset
Foggy lane detection
Global attention
Edge enhancement

ABSTRACT

Lane detection is a critical component of Advanced Driver Assistance Systems (ADAS). Existing lane detection algorithms generally perform well under favorable weather conditions. However, their performance degrades significantly in adverse conditions, such as fog, which increases the risk of traffic accidents. This challenge is compounded by the lack of specialized datasets and methods designed for foggy environments. To address this, we introduce the FoggyLane dataset, captured in real-world foggy scenarios, and synthesize two additional datasets, FoggyCULane and FoggyTusimple, from existing popular lane detection datasets. Furthermore, we propose a robust Fog-Enhanced Network for lane detection, incorporating a Global Feature Fusion Module (GFFM) to capture global relationships in foggy images, a Kernel Feature Fusion Module (KFFM) to model the structural and positional relationships of lane instances, and a Low-level Edge Enhanced Module (LEEM) to address missing edge details in foggy conditions. Comprehensive experiments demonstrate that our method achieves state-of-the-art performance, with F1-scores of 95.04 on FoggyLane, 79.85 on FoggyCULane, and 96.95 on FoggyTusimple. Additionally, with TensorRT acceleration, the method reaches a processing speed of 38.4 FPS on the NVIDIA Jetson AGX Orin, confirming its real-time capabilities and robustness in foggy environments.

1. Introduction

Lane detection plays an important role in Advanced Driver Assistance Systems (ADAS), providing essential support for lane keeping, autonomous navigation, and lane departure warnings, which help reduce the risk of lane-deviation accidents. As intelligent driving technologies advance, the need for robust and real-time lane detection in complex road environments is becoming more apparent, making it a key research focus in autonomous driving.

Under good weather and clear lane markings, current lane detection algorithms perform well. However, in complex road environments and poor weather, such as fog, lane markings can become blurred, image quality may decrease, and global environmental information is often obscured, which makes lane detection more challenging. In these conditions, existing algorithms often struggle and may fail, leading to an increased risk of traffic accidents with more severe consequences[1]. Ensuring safe driving in these conditions calls for the development of high-precision, highly robust lane detection methods optimized for foggy environments. As shown in Fig. 1, the in-vehicle camera captures real-time road images, which are preprocessed by edge devices and then sent to the lane detection module. Detected lane information is fused with data from other sensors, such as radar and GPS, along with real-time traffic data from the

*This project is jointly supported by National Natural Science Foundation of China (Nos. 52172350, W2421069 and 51775565), the Guangdong Basic and Applied Research Foundation (No. 2022B1515120072), the Guangzhou Science and Technology Plan Project (No. 2024B01W0079), the Nansha Key RD Program (No. 2022ZD014), the Science and Technology Planning Project of Guangdong Province (No. 2023B1212060029).

*Corresponding author

✉ zhangrh25@mail.sysu.edu.cn (R. Zhang); mayh39@mail2.sysu.edu.cn (Y. Ma); litf23@mail2.sysu.edu.cn (T. Li); linzy88@mail2.sysu.edu.cn (Z. Lin); wuyy236@mail2.sysu.edu.cn (Y. Wu); chenjunzhou@mail.sysu.edu.cn (J. Chen); tongjizl@tongji.edu.cn (L. Zhang); hujia@tongji.edu.cn (J. Hu); zhijunqiu@ualberta.ca (T.Z. Qiu); guokh@jlu.edu.cn (K. Guo)

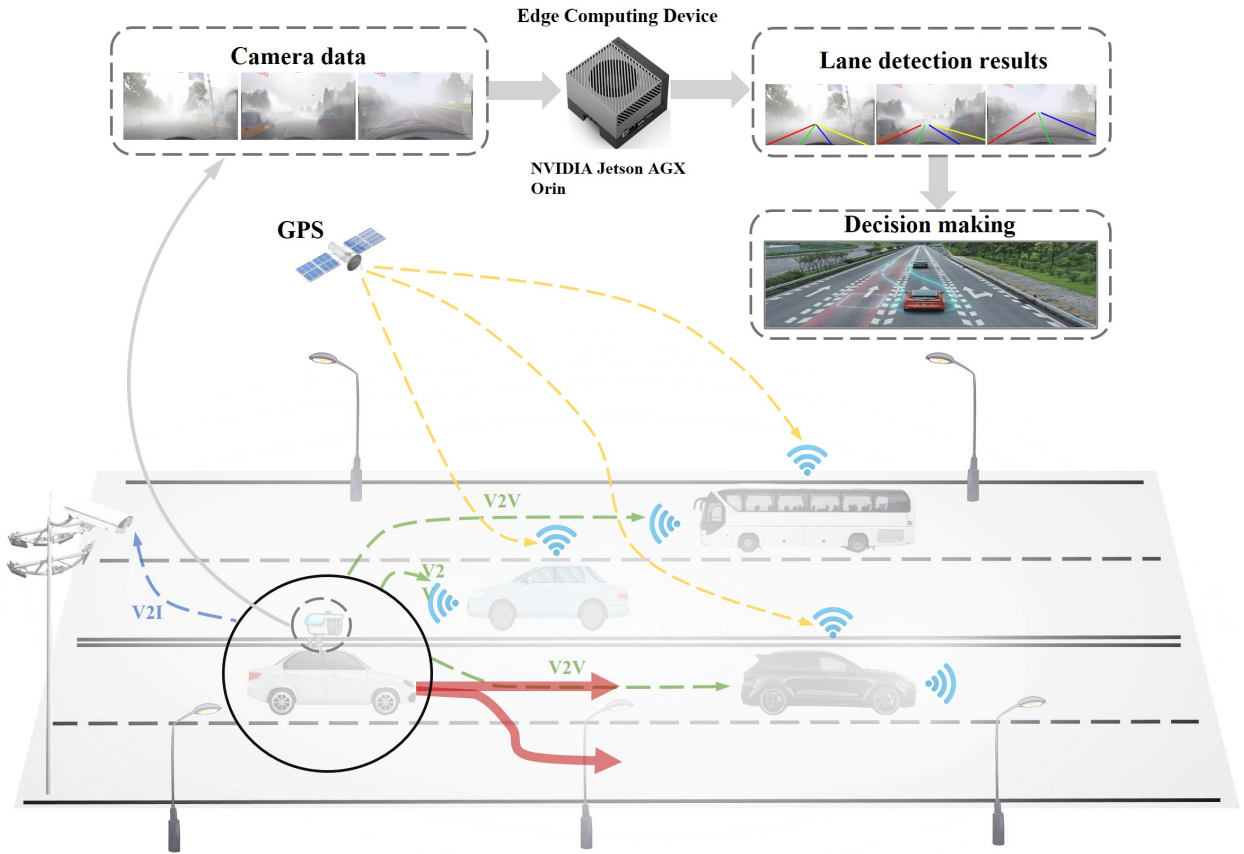


Figure 1: Lane detection in foggy scenarios for ADAS.[5]

cloud. This information is processed in the vehicle's computing unit, allowing the system to make adaptive driving decisions such as accelerating, braking, or steering[2, 3] to ensure safety in challenging environments like fog.

Although end-to-end autonomous driving technologies have made significant progress at Level 3 (L3) and higher, most current vehicles, particularly commercial and urban vehicles, are still at Level 0 (L0), Level 1 (L1), and Level 2 (L2). In these lower levels of autonomous driving, lane detection remains a crucial technology, especially in complex and adverse road environments. Most existing vehicles rely on Advanced Driver Assistance Systems (ADAS) to enhance safety in complex scenarios, especially in active warning, lane-keeping, and other functions[4]. Therefore, this research not only focuses on end-to-end autonomous driving technologies but also aims to improve lane detection performance in complex environments, providing stronger safety support and driving assistance for L0, L1, and L2 vehicles in adverse conditions.

Earlier lane detection algorithms were mainly based on traditional computer vision methods, typically including three steps: image preprocessing, feature extraction, and lane model fitting. Son et al.[6] first detected the vanishing point to adaptively select the ROI, then extracted lane markings based on color features, followed by clustering to find the main lane. Hou et al.[7] used the Canny operator to extract lane edges, filtered out noise with abnormal directions, and applied a progressive probabilistic Hough transform for line detection, filtering out unwanted lines with vanishing point constraints. These feature-based methods are simple, efficient, and suitable for real-time applications, but they also have clear limitations, such as requiring manual parameter tuning and high dependence on clear lane edges. When lane markings are worn, obscured, or subject to environmental changes, accurate detection becomes challenging, and robustness is limited. Improving and optimizing these methods remains necessary to enhance their robustness and adaptability for practical use.

Owing to the rapid development of deep learning, it has been widely applied in various autonomous driving tasks. For example, in traffic object detection, Wang and Zhang[8] proposed CRRFNet, an adaptive method that combines camera and radar fusion, improving detection accuracy and robustness in noisy or abnormal scenes. In accident detection and classification, Yang et al.[9] developed a deep learning model that utilizes multi-vehicle trajectory data for detecting and classifying accidents on freeways, achieving up to 100% detection accuracy. For 3D object detection under adverse weather, Qi et al.[10] introduced a novel geometric information constraint network (GIC-Net), enhancing the performance of 3D object detection by incorporating geometric location and line feature constraints, demonstrating superior results under challenging weather conditions. In addition to these applications, lane detection has also seen significant advancements, with deep learning-based approaches becoming mainstream due to their strong feature extraction capabilities and generalization. Compared to traditional methods, deep learning provides higher robustness, better adapting to complex road environments and effectively handling cases with missing or occluded lane markings. LaneNet[11] approaches lane detection as a combination of semantic segmentation and post-processing, first generating a semantic segmentation map of the lanes and then using density clustering to identify each lane instance. However, because of the large number of pixels generated during segmentation and the inability of clustering to leverage GPU acceleration, its real-time performance remains limited. LaneAF[12], building on the semantic segmentation map, introduced a clustering algorithm based on horizontal and vertical vector fields to accelerate post-processing and used DLA[13] as the backbone network to integrate multi-level semantic and spatial information, enhancing feature representation. SCNN[14] leveraged the elongated structure of lane lines by replacing traditional layer-wise convolution with slice convolution, enabling cross-row and cross-column information transfer, which makes it well-suited to line-like lane structures. However, its large parameter size prevents real-time performance. Overall, current networks, whether for semantic or instance segmentation, mostly rely on pixel-by-pixel classification, though lane detection does not necessarily require dense pixel segmentation. To address this, Qin et al.[15] reframed lane detection as a row-based segmentation problem using global features, significantly reducing computational cost and improving detection speed by selecting specific rows and classifying each pixel in the row. This method also leverages the large receptive field of global features, enabling it to handle complex scenarios with missing or occluded lanes.

Apart from segmentation, lane detection also includes detection-based methods, many of which borrow the Anchor-based Methods from object detection[16, 17, 18, 19]. However, due to the elongated shape of lane lines, traditional bounding boxes are not ideal. In lane detection, anchors are often a series of preset starting points and straight lines with different slopes, represented as point sets, with the network predicting the relative distance between the lane line and anchor to optimize line shape and position. PointLaneNet[20] first represents lane lines as a series of points, taking the intersections of evenly spaced horizontal lines as coordinates $\{x_1, x_2, \dots, x_n\}$ to describe the lane. Like other YOLO-based methods[16, 17], PointLaneNet divides the image into multiple grids, predicts lane position and classification at each grid center, and removes duplicate predictions through post-processing. However, this grid-based prediction approach has limitations for elongated lanes, reducing detection accuracy. LaneATT[21] addresses this issue by noting the high correlation between lane positions and introducing global features to infer lane position, especially in cases of occlusion or missing lane markers. LaneATT[21] introduced an anchor-based attention mechanism that significantly improves detection speed and accuracy by utilizing global information. CLRNet[22] demonstrated the complementary roles of low- and high-dimensional features in lane detection, proposing Cross Layer Refinement (CLR) to dynamically adjust anchor points through network learning, removing the limitations of fixed anchors to optimize lane detection further. FLAMNet[23] proposes an adaptive line anchor framework integrated with a dual-branch network design to improve the accuracy and adaptability of capturing intricate lane geometries. By leveraging the Decomposed Self-Attention (DSA) mechanism alongside a Horizontal Feature Fusion Module (HFFM), the model enhances the perceptual range of line anchors in lane detection tasks. This approach strengthens robustness against occlusions and incomplete lane markings in challenging environments.

In addition to these methods, trajectory data has also been explored for lane identification. Zhao and Roncoli[24] proposed a constrained spectral clustering method to identify lane information from high-resolution trajectory data, significantly improving results even in the presence of varying lane numbers or lane-changing maneuvers. This approach demonstrates the potential of leveraging trajectory data for lane detection, especially in more dynamic environments.

Compared to other detection and segmentation tasks, research on downstream tasks in adverse weather conditions, such as fog, is relatively limited. A conventional solution often applies standard image enhancement techniques, such as classical dehazing methods developed for fog removal and visual quality improvement. Nevertheless, enhanced visual clarity doesn't always correlate with superior detection outcomes. Some methods combine image enhancement with

detection to reduce adverse weather interference. Huang et al.[25] proposed DSNet, incorporating a detection subnet and recovery subnet, where multi-task learning combines dehazing and detection to improve understanding of foggy scenes, resulting in better detection than a standard detection network. Additionally, some methods simulate foggy images from existing datasets to optimize downstream tasks. For example, Nie et al.[26] used the Monodepth2 model and atmospheric scattering model to convert clear lane images from the CULane dataset into foggy lane images, achieving synthetic data augmentation. Testing with SCNN[14] showed that this augmentation strategy improved recognition rates from 76.65% to 86.65% under light fog conditions.

Another approach employs domain adaptation techniques to address the style gap between foggy scenes and clear-weather images[27, 28]. Hnewa et al.[29] assumed that there is domain shift between images captured in normal and adverse weather conditions, proposing a multi-scale domain-adaptive YOLO that supports domain adaptation at different levels in the feature extraction stage. Li et al.[30] proposed a novel transfer learning-based framework for fog-adaptive object detection, which integrates dual-level adaptation (image-level and object-level) to mitigate domain shifts caused by foggy conditions. Notably, the method only requires labeled clear-weather images and unlabeled foggy data for training, eliminating the dependency on annotated foggy datasets.

Traditional dehazing methods, which are based on statistical or physical principles, often suffer from artifacts such as image darkening or brightening. In contrast, end-to-end deep learning methods using Convolutional Neural Networks (CNNs) can capture more complex features but come with higher computational and memory demands. These methods are also highly dependent on diverse training datasets. However, acquiring real paired images under foggy conditions is challenging, and as a result, many existing datasets rely on synthetic images, which can negatively affect algorithm performance in real-world scenarios.

Lane detection is a critical component of Advanced Driver Assistance Systems (ADAS), supporting key functionalities such as lane departure warnings and autonomous navigation. While existing lane detection algorithms perform well under clear weather conditions with visible lane markings, their performance drops significantly in adverse environments like fog, where reduced visibility and image degradation obscure lane clarity, thus increasing the risk of traffic accidents. Furthermore, the lack of specialized datasets tailored to foggy conditions has limited the development of effective deep learning-based solutions for these challenging scenarios.

To address these limitations, we introduce the FoggyLane dataset, a new benchmark specifically designed for lane detection under foggy conditions. This dataset, comprising 1,423 annotated images across six distinct foggy road scenarios, fills a crucial gap in the current lane detection datasets. In addition, we generate foggy versions of two widely-used lane detection datasets, CULane [14] and Tusimple [31], creating FoggyCULane and FoggyTusimple datasets. These datasets are essential for training and testing lane detection algorithms in foggy environments.

In response to the unique challenges posed by foggy conditions, we propose a robust real-time lane detection method optimized for such environments. The main contributions of our work are as follows:

- 1) To address the issue of missing global information in foggy images, we design a Global Feature Fusion Module (GFFM) within the backbone network to capture relationships between inputs, improving feature extraction in foggy scenarios.
- 2) To enhance the utilization of structural relationships between lane instances, we introduce a Kernel Feature Fusion Module (KFFM) that learns and predicts the correlations between lane instances, improving lane detection accuracy and robustness.
- 3) To tackle the loss of edge information in foggy images, we incorporate a Low-level Edge Enhancement Module (LEEM) that enhances the model's attention to edge features, improving the accuracy and stability of lane detection.
- 4) To address the lack of open-source foggy lane detection datasets, we construct FoggyLane, a real-world dataset with 1,423 annotated images, and generate FoggyCULane and FoggyTusimple based on existing datasets. Our method achieves state-of-the-art performance with inference speeds of 192.9 FPS on NVIDIA RTX 3090 and 38.4 FPS on NVIDIA Jetson AGX Orin, confirming its real-time capability and practical applicability in real-world settings.

2. Related Work

In recent years, advances in deep learning have substantially improved lane detection performance. Building on these advances, current approaches for lane detection can be categorized into four main paradigms based on their modeling principles: segmentation-based, anchor-based, curve-based, and row-wise-based methods.

2.1. Segmentation-based Lane Detection

Segmentation-based methods mainly utilize semantic segmentation or instance segmentation techniques to distinguish lane lines from other objects or backgrounds in the image, transforming lane detection into a pixel-level classification problem. LaneNet[11] employs a two-branch structure of split branches and embedded branches, the split branches output a binary lane mask to recognize lane lines, and the embedded branches assign a unique embedding to each pixel to realize the distinction of lane lines. SCNN[14] extends the traditional layer-by-layer convolution operation with a slice-by-slice convolution operation, which passes the information horizontally and vertically between the pixels within a layer, thus enhancing the continuity of lane line recognition. RESA[32] introduces a spatial attention module that ensures robust lane prediction by cyclically shifting the feature map horizontally and vertically so that each pixel can acquire global information. Although these segmentation-based methods possess high accuracy and robustness, the models are bulky and slow to process due to high consumption of computational resources.

2.2. Curve-based Lane Detection

Curve-based methods transform the lane detection into a regression task by predicting polynomial coefficients that fit lane lines to polynomial equations. PolyLaneNet[33] introduces an end-to-end convolutional neural architecture that maps from images to polynomials representing each lane marker in the image, as well as domain lane polynomials and confidence scores for each lane. LSTR[34] can also directly output the parameters of the lane shape model, has developed a Transformer-based network that takes into account non-local interactions, enabling it to capture the narrow structure of the lane lines and global context information. DBNet[35] introduces NURBS curves and utilizes their geometric semantic properties to achieve local and global optimization, which improves the robustness of lane line detection and model interpretation. However, polynomial fitting is sensitive to parameter selection, and minor changes in parameters can result in significant variations in fitting results, leading to unstable lane line detection.

2.3. Anchor-based Lane Detection

Anchor-based approaches employ predetermined reference lines within the image space to generate lane predictions, subsequently calculating necessary offsets to precisely match these anchors with true lane markings. LineCNN[36] introduces the anchor mechanism into lane detection for the first time, and innovatively proposes line anchors. LaneATT[21] effectively solves the problem of occlusion and illumination due to the lack of a line anchor, by fusing extracted anchor features with global features generated by attention module. CLRNet[22] employs a coarse-to-fine detection strategy, where lane lines are first approximated using high-level semantic cues before being refined with detailed low-level features. This hierarchical fusion of semantic information significantly improves detection precision. FLAMNet[23] employs an adaptive line anchor strategy, augmented by patch-based feature pooling and decomposed self-attention mechanisms. This design strengthens both local feature extraction and global context modeling, improving performance in handling intricate lane structures. However, due to the multiple curvature and orientation variations of lane lines in the real world, the performance of the anchor-based methods may be limited in capturing precise paths with complex shapes.

2.4. Row-wise-based Lane Detection

Row-wise methods predict lane positions for each image row. E2E-LMD[37] first proposes the row-wise-based lane detection task and designs an end-to-end architecture that directly outputs the lane marker positions. UFLD[15] utilizes global features to select the lane positions of predefined rows of an image and proposes a structural loss function, so as to ensure the continuity and smoothness of the lanes. CondLaneNet[38] utilizes conditional convolution and row-by-row prediction strategies to enhance lane recognition accuracy, and introduces the RIM module to effectively address complex lane layouts. The row-wise-based detection methods improve computational efficiency by focusing only on the row regions in the image, and possesses high detection accuracy while maintaining efficiency.

3. Data Constrution

Due to the data-driven nature of deep learning models, the quality, size, and diversity of the datasets largely determine the applicability and performance of such models. In the task of lane detection, models trained solely on clear weather data struggle to adapt to low-visibility foggy conditions. Issues such as blurred lane boundaries, faded lane colors, and reduced image quality often arise in fog, making lane detection more challenging. Therefore, training with a foggy weather lane dataset can significantly improve an autonomous driving system's ability to handle such conditions, enhancing both detection accuracy and overall reliability. However, there is currently no publicly available foggy weather lane detection dataset. To address this gap, we have collected and constructed a foggy weather lane detection dataset called FoggyLane. In addition, we generated two supplementary datasets, FoggyCULane and FoggyTusimple, by using fog modeling techniques on existing CULane [14] and Tusimple [31] datasets to test the generalizability of our methods.

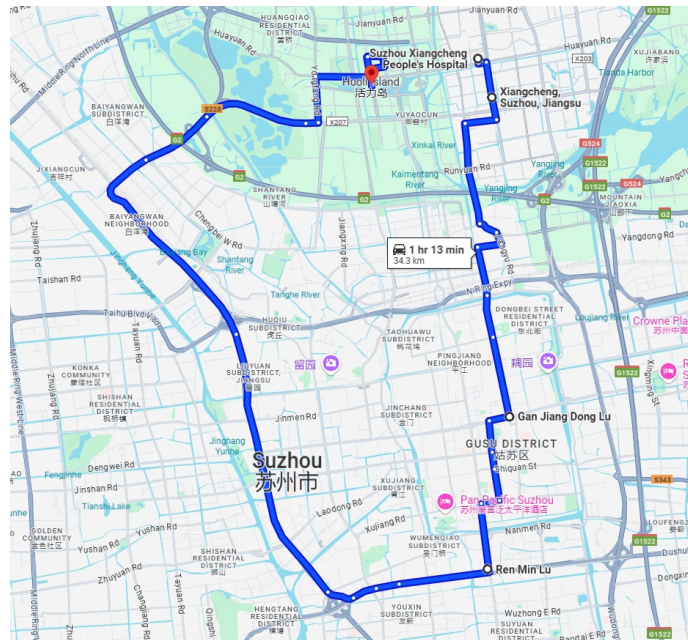


Figure 2: The route for dataset acquisition in Suzhou on the morning of October 26, 2023.[39]

3.1. FoggyLane

In the field of intelligent connected vehicle ADAS systems, existing lane detection algorithms have shown good performance under favorable weather conditions. However, their performance remains significantly inadequate under adverse weather conditions, such as fog. Given that fog is a high-risk scenario for traffic accidents, the limited visibility drastically reduces the driver's reaction time and decision-making ability, making accidents more likely. However, current benchmark datasets for lane detection, including CULane[14], Tusimple[31], and LLAMAS[40], do not include data from foggy scenarios. To address this gap, we have developed a lane detection dataset, FoggyLane, specifically designed for foggy conditions. Given the randomness of foggy weather, data collection was carried out using a monocular forward-facing camera at different times and locations. This includes the morning of October 26, 2023, in Suzhou, Jiangsu Province, China, and two sessions in Urumqi, Xinjiang Uygur Autonomous Region, China: the morning of December 9, 2023, and the night of January 2, 2024. In these selected representative traffic scenarios, we sampled one frame every frames, resulting in a total of 1,086 RGB images: 444 images (resolution: 1920×1080), 102 images (resolution: 2560×1920), and 540 images (resolution: 2304×1296). To simplify operations and enhance usability during training, we resized all images to a uniform resolution of 1640×590 .

However, since the duration of foggy weather conditions is limited, the number of collected foggy weather images is restricted. To improve the model's performance, we extended our dataset by incorporating additional foggy driving scenes. Specifically, we downloaded two foggy driving videos from YouTube[41], extracting road-driving segments at

Table 1
Comparison Between Our Dataset and Existing Lane Detection Datasets

Dataset	Frames	Multi-traffic scenarios	Instance-level annotation	Number of foggy datasets	Resolution
Caltech-Lanes [42]	1.2k	✗	✓	None	640 × 480
Tusimple [31]	6.4k	✗	✓	None	1280 × 720
LLAMAS [40]	100k	✓	✓	None	1276 × 717
Appolloscape [43]	110k	✓	✗	None	3384 × 2710
BDD100k [44]	100k	✓	✗	None	1280 × 720
CULane [14]	133k	✓	✓	None	1640 × 590
CurveLanes [45]	150k	✓	✓	None	1280 × 720
FoggyLane (ours)	1.5k	✓	✓	1.5k	1640 × 590

20-frame intervals, obtaining 44 and 293 frames, respectively. This added a total of 337 additional RGB images to the dataset. The original resolution of these images was 1920×1080 , and they were resized to 1640×590 for consistency.

As a result, we have constructed FoggyLane, a foggy weather lane detection dataset consisting of 1,423 images. FoggyLane includes six types of road scenes, as shown in Fig. 4, covering Normal, Arrow, Crowd, Curve, Night and Crossroad. We split the dataset into training and testing sets at a ratio of 2:1. To ensure comprehensive learning of scene characteristics, each type of scene is evenly distributed between the training and testing sets to maintain balance.

Meanwhile, We compared FoggyLane with existing lane detection datasets. As shown in Table 1, the Caltech-Lanes and Tusimple datasets only cover single traffic scenarios. The LLAMAS [40] dataset focuses on highway scenarios, but its annotations are generated from high-precision maps rather than manually annotated. While the ApolloScape [43] and BDD100k [44] datasets contain multiple traffic scenarios, they lack instance-level annotations, and ApolloScape [43] does not provide publicly available test set annotations. In comparison, although CULane [14] and CurveLanes [45] include a wide range of traffic scenes with comprehensive annotations, they still lack foggy weather scenarios. For lane detection tasks, models trained only on clear weather conditions struggle to handle the challenges posed by fog, such as blurred lane boundaries, faded colors, and reduced image quality. To address these limitations, we developed FoggyLane, a comprehensive foggy weather lane detection dataset that includes 1,423 images featuring various challenging scenarios such as foggy roads during the day, curves, crossroads, and night fog. The dataset is meticulously annotated using the LabelMe tool, providing instance-level annotations, and it is available in Tusimple [31] and CULane [14] formats for broader accessibility.

Our dataset has two key advantages:

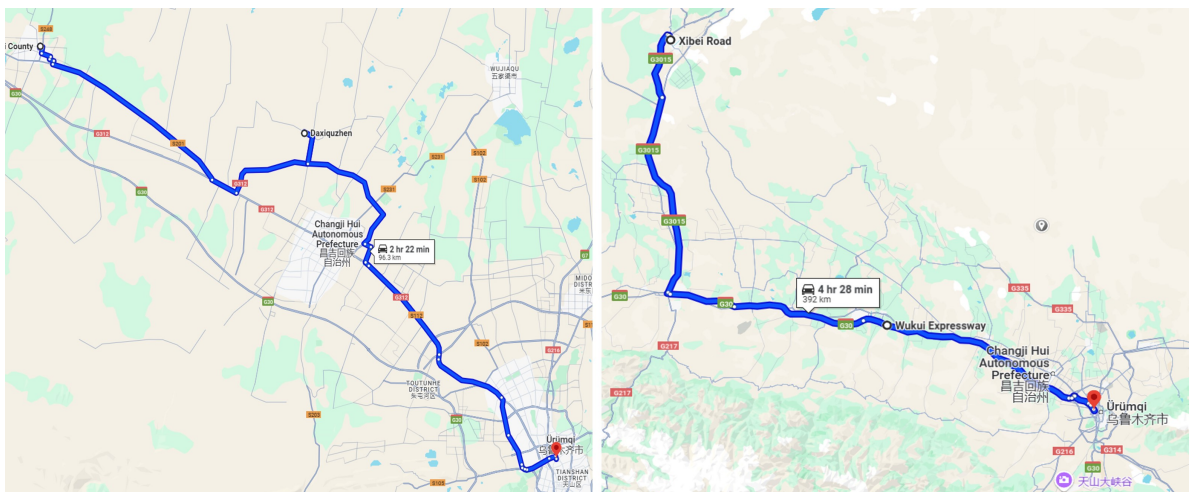


Figure 3: The routes for dataset acquisition in Urumqi, Xinjiang Autonomous Region: the left illustrates the morning of December 9, 2023, while the right depicts the evening of January 2, 2024.[39]

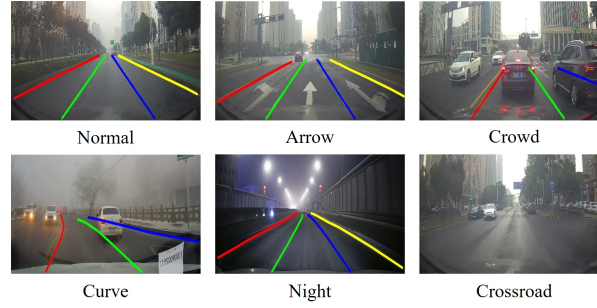


Figure 4: The different road types of FoggyLane images examples.

- 1) Pioneering foggy lane detection dataset: FoggyLane is a dataset specifically designed to address foggy weather scenarios. It covers a range of challenging conditions, including foggy congested roads, foggy curves, and foggy night roads. This dataset is crucial for testing the robustness of ADAS under adverse conditions.
- 2) Strict annotation standards: The dataset follows strict annotation guidelines, including marking the center of lanes, connecting lane markings at intersections, and prioritizing solid lines over grid lines, etc.[46]. These rigorous annotations can significantly improve the accuracy and consistency of lane detection in foggy weather, thus enhancing the stability and safety of autonomous driving systems and providing a solid data foundation for the reliable deployment of autonomous technology.

3.2. FoggyCULane and FoggyTusimple

Currently, numerous datasets are available for lane detection. Among them, we select two widely adopted and representative benchmarks: CULane[14] and TuSimple[31]. The CULane dataset [14] is a large-scale and challenging benchmark that covers diverse scenarios including highways, urban streets, and rural areas in Beijing. In contrast, the TuSimple dataset [31] primarily comprises daytime driving videos collected on American highways, featuring a variety of lighting conditions and complex traffic situations. Based on these datasets, we generate synthetic foggy versions, named FoggyCULane and FoggyTuSimple, to facilitate evaluation under adverse weather conditions.

The method for generating foggy images is inspired by the model [26], and the complete generation process is shown in Fig. 5. To be specific, the atmospheric scattering model can effectively utilize prior information to analyze the degradation mechanisms of image quality in foggy conditions. It models foggy images as a combination of scattered light and direct light based on optical principles, ultimately synthesizing a clear image into a foggy one. The mathematical modeling equation defined by Koschmieder[47] is represented as:

$$I(x) = J(x)t(x) + A(1 - t(x)) \quad (1)$$

where x indicates a certain pixel of the image, $J(x)$ refers to the original clear image of the object and $I(x)$ refers to the foggy image. A is the atmospheric light value at infinity and $t(x)$ can be further defined as:

$$t(x) = e^{-\beta d(x)} \quad (2)$$

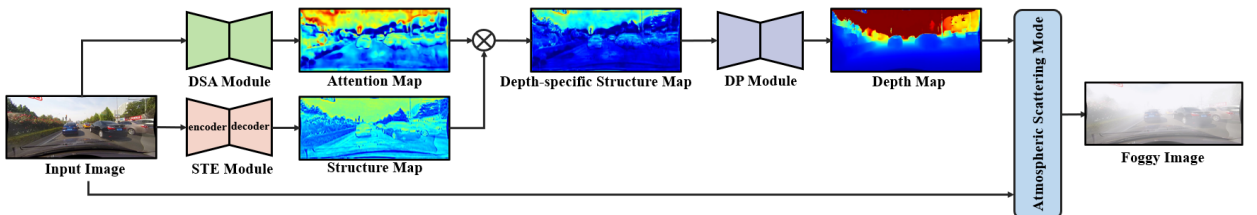


Figure 5: Networks of foggy image generation. \otimes represents element-wise multiplication.

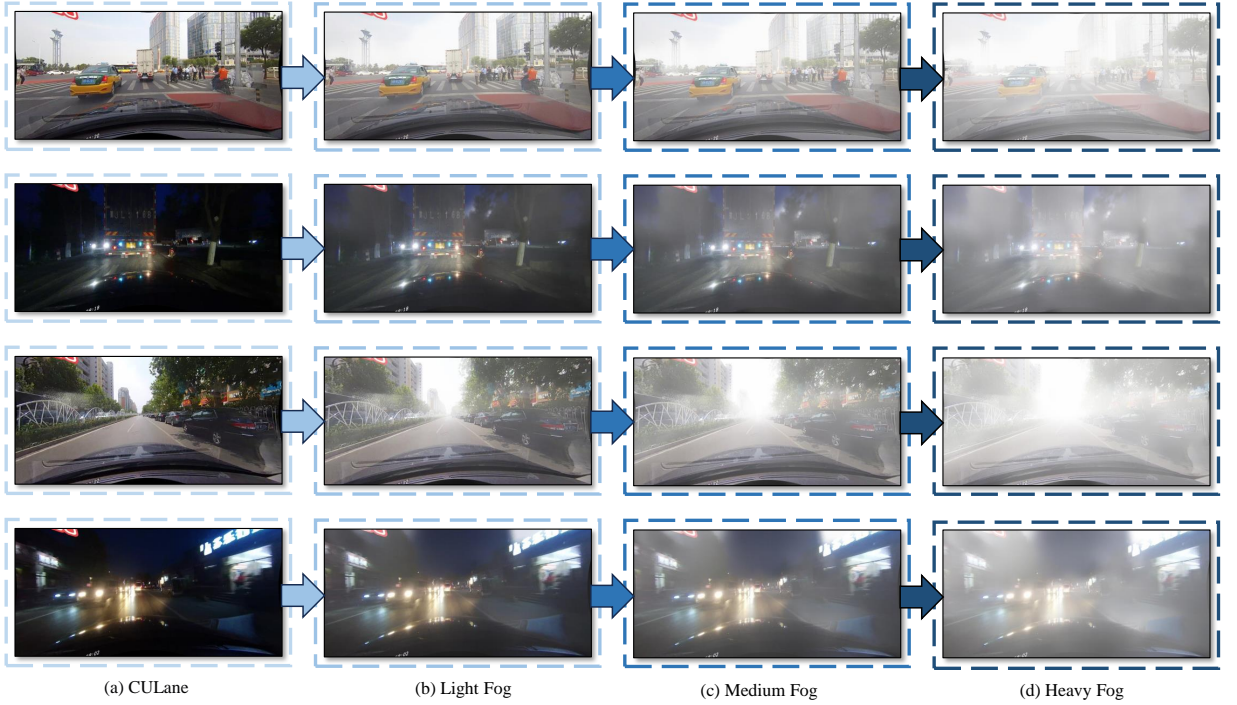


Figure 6: The FoggyCULane dataset examples. (a) is the original CULane dataset. And (b) to (d) are the foggy images of different concentrations with β values of 2, 4, and 8, respectively.

where β is the extinction coefficient, which is closely related to the concentration, size, type and distribution of particulate matter. $d(x)$ represents the distance between the object and the viewer. As this distance increases, the transmittance decreases, resulting in thicker fog. To calculate the corresponding $d(x)$, we use the S2R-DepthNet[48] that has good generalization performance across various applications. The S2R-DepthNet consists of three modules that decouple the structural and textural information of the input image. Then they suppress information irrelevant to depth and use structural information for depth prediction. The Structure Extraction Module (STE) decomposes the image to obtain domain-invariant structure information. The Depth-specific Attention (DSA) predicts an attention map that helps to suppress depth-irrelevant structures by leveraging high-level semantic information extracted from the raw image. After passing through the DSA Module and STE Module, as shown in Fig. 5, the attention map and the structure map are multiplied to obtain a concise and comprehensive depth-specific structure map. The Depth Prediction (DP) is responsible for depth estimation. According to the transmittance formula Eq. (2), we use the dark channel prior[49] to calculate the average atmospheric light value A . In the non-sky area of an outdoor clear image, there is usually at least one very small or close to zero value in the RGB image for each pixel, which is called the dark channel of that pixel. Therefore, for any image I , the mathematical formula for its corresponding dark channel image $I_{\text{dark}}(x)$ can be defined as:

$$I_{\text{dark}}(x) = \min_{c \in R, G, B} \left(\min_{y \in \Omega(x)} I_c(y) \right) \quad (3)$$

where $I_c(y)$ is the value of the c -th channel of image I at pixel point y , and $\omega(x)$ is a small region around pixel point x . In the dark channel, find the top 0.1% brightest pixels and take the maximum value of their RGB channels as an approximation of the average atmospheric light value A . After obtaining the transmittance and the average atmospheric light value, the images of light fog, medium fog, and heavy fog can be obtained by fine-tuning the extinction coefficient β . The original images and the foggy images generated under different β values are displayed in Figs. 6 and 7.

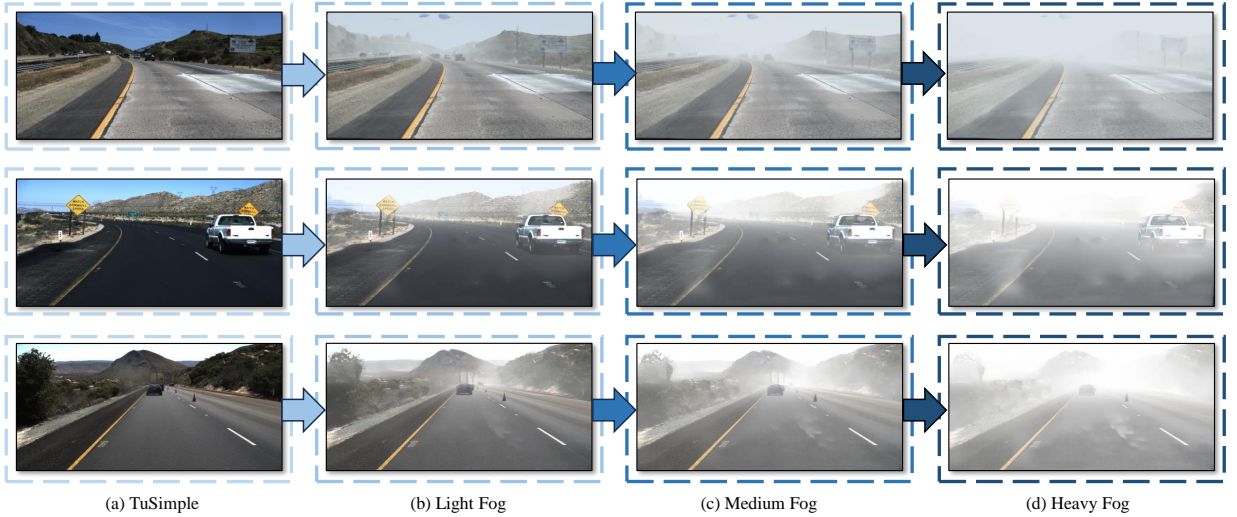


Figure 7: The FoggyTuSimple dataset examples. (a) is the original TuSimple dataset. And (b) to (d) are the foggy images of different concentrations with β values of 2, 4, and 8, respectively.

4. Methods

4.1. Overall structure

To address the challenge of lane detection in foggy conditions, where visibility is significantly reduced, we propose a fog-enhanced lane detection network inspired by row-wise methods. As illustrated in the Fig. 8, the network comprises three main components: a backbone network, a neck network, and a detection head. To mitigate the loss of global information in foggy images, we introduce a global feature fusion module within the backbone network. In the neck network, we utilize HRNetV2[50] to further integrate multi-scale features from different stages of the backbone, enabling the aggregation of information across various scales and resolutions.

For the detection head, we employ the concept of dynamic convolution, incorporating both lane instance detection and lane mask segmentation. During instance detection, the network identifies lane instances within the image and predicts a set of dynamic convolution kernel parameters for each lane. These parameters are subsequently applied to the lane mask segmentation head to filter the instance-specific segmentation map for each lane. This approach eliminates the need for complex post-processing steps, enhancing detection speed.

Moreover, to fully exploit the structural relationships between lane lines, we designed a kernel feature fusion module, which allows the network to automatically learn the correlations between predicted lane instances. This contributes to more accurate lane identification and localization. Additionally, to compensate for the loss of edge information in foggy images, we incorporated a low-level edge enhancement module, further improving the network's ability to detect lane boundaries with precision.

4.2. Global Feature Fusion Module

In recent years, Transformer models have achieved significant success in natural language processing, leading researchers to explore their applications in computer vision. With self-attention mechanisms, Transformer models can capture dependencies between different regions and pixels within an image, thus facilitating a better understanding of global image information. As a result, Transformer models have demonstrated outstanding modeling capabilities and performance improvements in various traffic vision tasks[51, 52, 53]. However, applying Transformers to the visual domain still faces some challenges. Firstly, traditional Transformer architectures lack the hierarchical structure and down-sampling operations found in CNN models, making them less adaptable to changes in resolution and receptive field, which may hinder handling of complex visual entities. Additionally, calculating global attention at high resolutions can be computationally intensive.

To address these issues, researchers have proposed several enhanced architectures, such as hierarchical Transformers [54, 55, 56]. Among them, the Swin Transformer[54] combines CNN-inspired concepts, integrating local

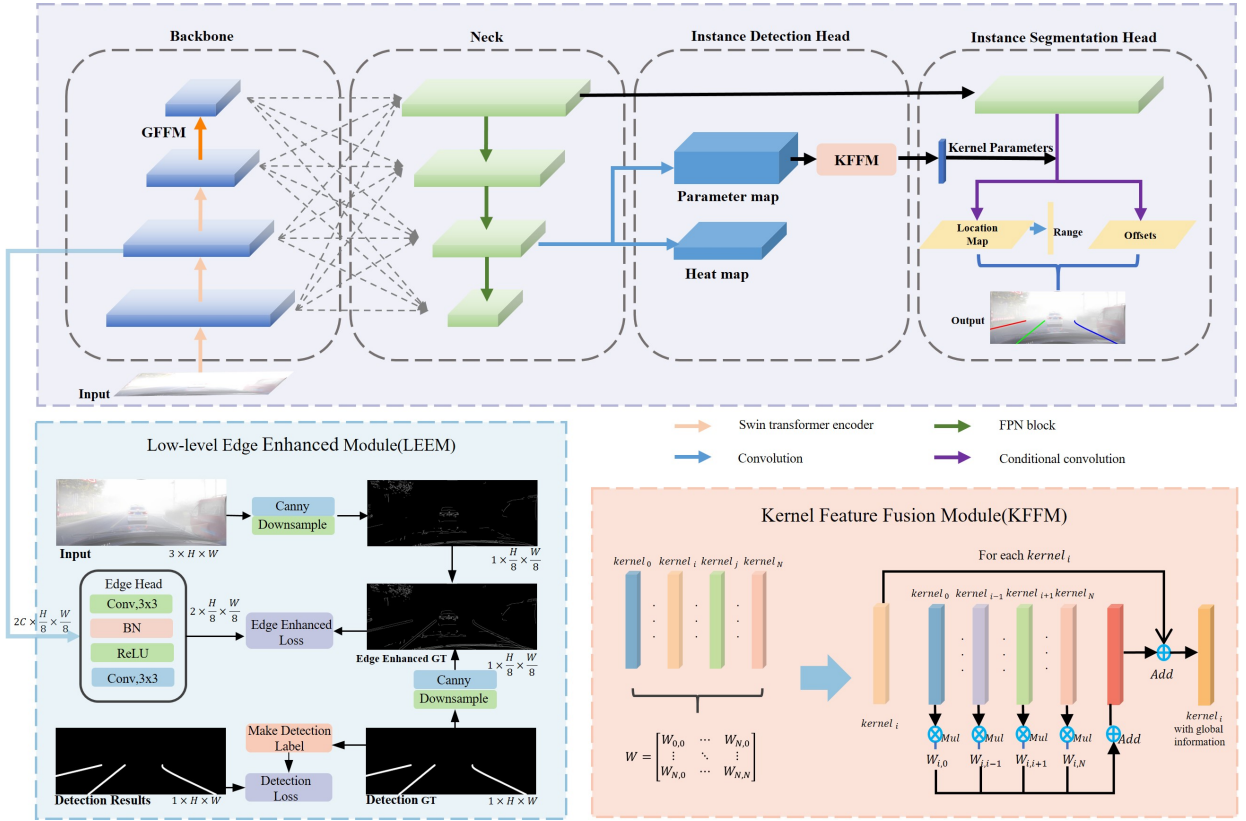


Figure 8: Overview of the proposed network.

perception with global attention in a hierarchical Transformer framework. By incorporating a sliding window approach similar to convolution, the Swin Transformer limits self-attention calculations within each sliding window, enabling local information interactions while reducing computational load and improving efficiency. The Swin Transformer also adopts a multi-scale hierarchical structure similar to that of CNNs, dividing the model into multiple stages. In each stage, a Patch Merging layer performs down-sampling to reduce the computational load, followed by the Swin Transformer Block, which applies self-attention within sliding windows. The Swin Transformer Block includes

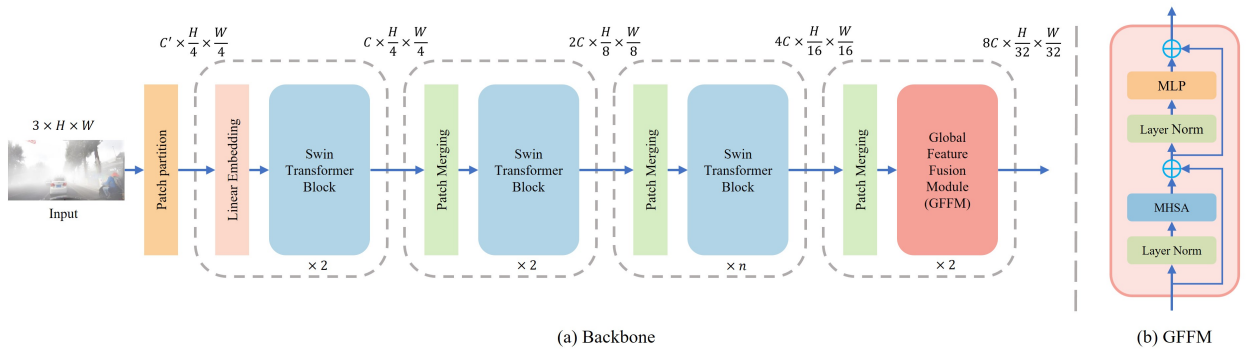


Figure 9: Backbone Network with Global Feature Fusion.

both Window Attention and Shifted Window Attention mechanisms; the former computes self-attention within each window, while the latter enables information exchange across windows.

The Swin Transformer has shown strong performance in classification, detection, and segmentation tasks, balancing computational efficiency with accuracy. Thus, we chose the Swin Transformer as our backbone network. However, since the Swin Transformer's window attention mechanism primarily focuses on local features, its hierarchical structure may still lack sufficient global context for foggy scene understanding. Therefore, as illustrated in the Fig. 9, we designed a Global Feature Fusion Module (GFFM) to enhance the network's global information integration. Specifically, we replaced the window attention mechanism in the final stage with a standard multi-head attention mechanism to capture global correlations across all inputs. At this stage, image resolution has been sufficiently reduced, making the computational cost of global attention manageable.

4.3. Kernel Feature Fusion Module

Dynamic convolution is a specialized convolution operation that dynamically adjusts kernel parameters based on the input data. In conventional convolutions, kernel parameters remain fixed after training and are independent of the input data. In contrast, dynamic convolution adapts kernel parameters for each input, enhancing the network's flexibility and generalization. For specific tasks, dynamic convolution often achieves better performance than standard convolution. CondInst[57] is an instance segmentation framework based on dynamic convolution, which generates convolution kernel parameters dynamically for each instance based on its features and applies them in the segmentation head to filter the instance's mask. Since each kernel parameter only needs to handle a single instance, this approach reduces the network's learning burden and convolutional computation load, while also eliminating the ROI operations required in methods like Mask R-CNN, creating a faster, more streamlined instance segmentation framework. Other frameworks, such as SOLO[58], SOLOv2[59], and CondLane[38], have also applied dynamic convolution in instance segmentation, with CondLane specifically designed for lane instance segmentation, achieving robust performance with its dynamic convolution-based lane detection strategy.

Building on these studies, our lane detection head also incorporates dynamic convolution. This detection head includes two components: lane instance detection and lane mask segmentation. During instance detection, the network identifies lane instances within the image and generates a set of dynamic convolution kernel parameters for each lane. These kernel parameters are applied in the lane mask segmentation head to isolate each lane's instance segmentation. In typical dynamic convolution-based instance segmentation frameworks, the center position features of each instance are used to generate the dynamic convolution kernels. However, for lane detection, this is less effective, as lanes are elongated structures, making it challenging for center features to capture information along the full lane length. Therefore, following CondLane's approach, we use the starting position features of each lane to guide the dynamic convolution kernel generation. Specifically, we design an instance detection head in the third stage of the neck network's feature map, comprising two branches: one branch predicts the starting points of lanes, generating a heatmap for these points; the other branch predicts a set of dynamic convolution kernels for each position, using the kernel at the lane's starting position for subsequent segmentation.

However, the existing method using lane starting points does not account for the inherent structural and positional relationships among lane instances. In a top-down view, lanes are often parallel, similar in shape, and have consistent spacing. To fully leverage this structural information, we designed a Kernel Feature Fusion Module (KFFM) to enable the network to automatically learn and predict relationships between lane instances. The KFFM is shown in the bottom right of the Fig. 8.

4.4. Low-level Edge Enhanced Module

Images in foggy conditions differ from those captured under good lighting primarily due to their blurriness and low contrast. This effect renders the edges of objects and details within the scene indistinct and hard to detect, impacting the algorithm's ability to understand and recognize the scene accurately. Edge information, beyond simply marking object boundaries, also implicitly contains structural and spatial information about objects, forming a critical foundation for tasks such as object detection, segmentation, and tracking. Using the Canny edge detection algorithm with identical threshold settings, we processed both foggy and normal images, as shown in the Fig. 10. It is evident that fog significantly degrades edge information, particularly affecting lane line edges, which become nearly indiscernible. Given that lane detection relies heavily on edge information—lane positioning is typically determined by the boundary between lane edges and the road background—both global scene information and detailed edge information are essential for accurate lane detection. To address the challenges of lane detection in foggy conditions, we apply global

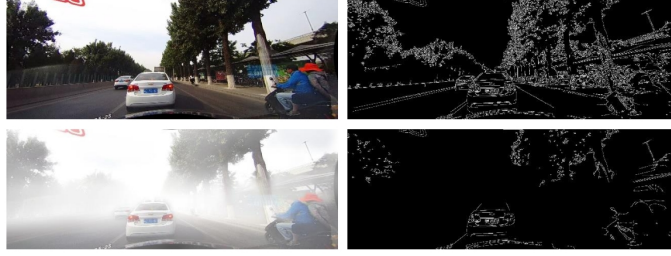


Figure 10: Comparison of edge information between foggy and normal scenarios.

feature fusion within both the backbone network and detection head to enhance high-dimensional global features. Additionally, we use multi-scale fusion to aggregate detail features from low-resolution feature maps. However, this approach alone does not fully compensate for the loss of edge detail inherent in foggy images. Therefore, we introduce a Low-level Edge Enhanced Module (LEEM) into the network to boost the network's focus on edge information, thereby improving both the accuracy and stability of lane detection.

Specifically, we add an auxiliary path in the network to learn the edge features of the input image. First, we apply the Canny operator to the input image for edge detection, supplemented by lane line labels to reconstruct any missing lane edges, generating the training labels for the edge enhancement module. To avoid interfering with high-level semantic extraction and subsequent detection segmentation, while strengthening the low-level network's learning of edge textures and other low-dimensional features, we introduce a branch at the second stage of the backbone network. This branch sequentially applies a 3×3 and a 1×1 convolution. We then compute the cross-entropy loss between the branch output and the edge labels. The detailed structure is illustrated in the bottom-left of the Fig. 8. Notably, this auxiliary enhancement path is only active during training, thus not increasing computation or processing time during deployment.

4.5. Loss functions

Based on the above, our method involves a total of five prediction tasks: lane start point prediction, row-based segmentation prediction, vertical range prediction, offset prediction, and edge prediction. The loss functions for each task are detailed below.

4.5.1. Lane start point prediction

In feature maps with a large receptive field and low resolution, the lane line start point is difficult to be accurately represented by a single pixel location. Moreover, in such large receptive field feature maps, pixels near the target point exhibit similar features. If these pixels are directly labeled as negative samples, it will interfere with the network training and make it difficult for the network to learn and optimize. Therefore, this method uses a Gaussian kernel function to generate a heatmap label for the lane line start point. Each element in the heatmap label represents the confidence that the position corresponds to the target point; the closer to the target point, the higher the confidence, and the farther away, the lower the confidence. In other words, the ground truth is softly labeled with a Gaussian function, making it easier for the network to converge. Suppose (x, y) denotes a position on the low-resolution feature map, and (p_x, p_y) represents the coordinate of the target point on the low-resolution feature map. Then, the ground truth heatmap GT value at position (x, y) is defined as:

$$GT(x, y) = \exp\left(-\frac{(x - p_x)^2 + (y - p_y)^2}{2\sigma^2}\right) \quad (4)$$

where σ controls the decay rate of the Gaussian kernel. A larger σ results in slower confidence decay and thus a larger heatmap area.

This method combines the Gaussian heatmaps of all lane line start points within the image into a single heatmap. When multiple heatmaps respond at the same location, the maximum value is retained to form the final ground truth heatmap. Then, the Focal Loss is used to calculate the loss between the predicted heatmap and the ground truth heatmap. Let the predicted heatmap value at position (x, y) be $P_{x,y}$, and let N be the total number of pixels in the heatmap. The Focal Loss between the predicted heatmap and the ground truth heatmap is defined as:

$$\mathcal{L}_{hm} = -\frac{1}{N} \sum_{x,y} \begin{cases} (1 - P_{xy})^\alpha \log(P_{xy}), & \text{if } GT(x, y) = 1 \\ (1 - GT(x, y))^\beta (P_{xy})^\alpha \log(1 - P_{xy}), & \text{otherwise} \end{cases} \quad (5)$$

4.5.2. Row-based segmentation prediction

Row-based segmentation predicts a horizontal coordinate $E(\hat{x}_i)$ for each row. For this task, our method uses the L1 loss function to optimize the predicted coordinates. Suppose V denotes the effective vertical range of the lane line, N_v is the number of effective rows, and x_i is the ground truth horizontal coordinate. The loss function is defined as:

$$L_{row} = \frac{1}{N_v} \sum_{i \in V} |E(\hat{x}_i) - x_i| \quad (6)$$

4.5.3. Vertical range prediction

For the label of the lane line vertical range vector prediction, our method uses a $1 \times Y$ vector representation. If the lane line passes through the Y_i row, its value is 1; otherwise, it is 0. Thus, this can be regarded as a segmentation task. Our method optimizes it using the cross-entropy loss function. Suppose v_i denotes the predicted probability that the i -th row is positive, then the loss function is defined as:

$$L_{range} = \sum \left(-y_{gt}^i \log(v_i) - (1 - y_{gt}^i) \log(1 - v_i) \right) \quad (7)$$

4.5.4. Offset prediction

Firstly, the generation of ground truth labels for offset prediction is required. For each lane line, the proposed method constructs the ground truth offset as the horizontal displacement relative to the lane centerline for each grid cell within a specified width. The predicted offsets are optimized using an L1 loss function. Let δ_{xy} denote the ground truth offset at coordinate (x, y) , $\hat{\delta}_{xy}$ the predicted offset, and Ω the region surrounding the lane line. The loss function is then formulated as follows:

$$L_{offset} = \frac{1}{N_\Omega} \sum_{(x,y) \in \Omega} |\hat{\delta}_{xy} - \delta_{xy}| \quad (8)$$

4.5.5. Edge prediction

For the task of edge enhancement, the method treats it as an edge segmentation problem, which is essentially a binary classification task. The labels at edge locations are assigned a value of 1, while non-edge locations are assigned 0. Accordingly, the cross-entropy loss function is employed for optimization. Let e_{gt}^i denote the label of pixel i , and p_i represent the predicted probability of the pixel being positive. The loss function is defined as:

$$L_{edge} = \sum_i \left(-e_{gt}^i \log(p_i) - (1 - e_{gt}^i) \log(1 - p_i) \right) \quad (9)$$

4.5.6. Total loss

To balance the influence of different tasks on the overall training of the network, a weighted fusion of the loss functions for each sub-task is employed. The total loss function is formulated as follows:

$$L_{total} = \alpha L_{hm} + \beta L_{row} + \gamma L_{range} + \delta L_{offset} + \epsilon L_{edge} \quad (10)$$

where the network achieves optimal performance when the weights are set as $\alpha = 1$, $\beta = 1$, $\gamma = 1$, $\delta = 0.4$, and $\epsilon = 0.1$.

5. Experiments

5.1. Datasets

In the Data Construction chapter, we introduce the FoggyLane dataset, which was constructed from real-world collections for foggy lane detection, along with the FoggyCULane and FoggyTusimple datasets that were synthesized through modeling foggy images. Our method is evaluated on these three datasets.

FoggyLane is a lane detection dataset specifically designed for foggy scenarios, containing 1,423 frames of foggy lane images for training and testing. All images are of resolution 1640×590 pixels.

FoggyCULane is synthesized from the large-scale challenging lane detection dataset CULane using a foggy image modeling approach. It maintains the same number of images as CULane, which includes 88,880 images for training and 34,680 images for testing. The resolution of all images is also 1640×590 pixels.

FoggyTusimple is synthesized from one of the most widely used benchmark datasets for lane detection, Tusimple, through the foggy image modeling method. At the same time, the dataset follows the same structure as Tusimple, comprising 3,268 training images, 358 validation samples, and 2,782 test cases. All visual data maintains a consistent resolution of 1280×720 pixels.

5.2. Evaluation Metric

Lane detection tasks are typically regarded as a semantic segmentation problem; therefore, the evaluation metrics for lane detection are often similar to those used in segmentation tasks, specifically the confusion matrix: TP (True Positive), FP (False Positive), FN (False Negative), and TN (True Negative). In the context of lane detection, TP typically represents the correctly predicted lane line pixels, FP denotes incorrectly predicted lane points, FN refers to lane line points that were not detected by the model but are actually present, and TN indicates correctly predicted background pixels. Furthermore, the nature of lane detection tasks introduces some unique characteristics that differentiate their evaluation criteria from those of standard segmentation tasks.

For FoggyLane and FoggyCULane, we adopt the evaluation metrics of SCNN[14], connecting the labeled or predicted lane points sequentially to form a long line segment with a width of 30 pixels centered around the connecting line. We then calculate the Intersection over Union (IoU) between the predicted area and the ground truth area. If the IoU of the predicted area and the ground truth area exceeds a certain threshold (typically set at 0.5), the lane detection is considered correct; otherwise, it is deemed incorrect. Based on this, we calculate the Precision, Recall, and F1-score, with the following formulas:

$$F1 = \frac{2 \times Precision \times Recall}{Precision + Recall} \quad (11)$$

$$Precision = \frac{TP}{TP + FP} \quad (12)$$

$$Recall = \frac{TP}{TP + FN} \quad (13)$$

For the FoggyTusimple dataset, we adopt the evaluation metrics of the Tusimple dataset. The official Tusimple dataset provides three standard evaluation metrics: false positive rate (FPR), false negative rate (FNR), and accuracy. The formula for calculating Accuracy is as follows:

$$Accuracy = \frac{\sum_{clip} C_{clip}}{\sum_{clip} S_{clip}} \quad (14)$$

where C_{clip} represents the number of correctly predicted lane points in the image, while S_{clip} denotes the total number of ground truth lane points. For the pixels in the image, a predicted lane point is considered correct if it falls within 20 pixels to the left or right of the ground truth. Furthermore, if more than 85% of the predicted lane points on a single lane line correspond to the ground truth lane points, the predicted lane is regarded as a true positive.

Table 2
Comparison with Advanced Lane Detection on FoggyLane dataset.

Method	Venue	Backbone	F1@050	F1@065	F1@075	F1@085	mF1	Gflops(G)	FPS
SCNN[14]	AAAI 2018	VGG16	84.01	62.08	56.34	12.76	41.78	328.4	18.7
UFLD[15]	ECCV 2020	ResNet18	81.76	56.54	32.32	6.50	38.24	8.4	327.3
UFLD[15]	ECCV 2020	ResNet34	82.75	61.25	34.44	7.89	40.23	16.9	176.9
LaneATT[21]	CVPR 2020	ResNet18	81.98	59.61	34.78	7.69	40.06	9.3	247.7
LaneATT[21]	CVPR 2020	ResNet34	84.32	63.08	38.91	10.76	42.63	18.0	167.1
LaneATT[21]	CVPR 2020	ResNet122	86.25	72.42	51.50	17.26	48.95	70.5	28.6
LSTR[34]	WACV 2021	ResNet34	83.79	68.23	58.29	25.32	48.91	-	124.4
RESA[32]	AAAI 2021	ResNet34	85.19	65.89	61.89	14.57	48.75	41.0	76.7
RESA[32]	AAAI 2021	ResNet50	86.24	69.22	65.27	16.55	52.34	43.0	53.0
CondLane[38]	ICCV 2021	ResNet18	90.38	75.08	47.50	47.50	10.96	10.2	194.7
CondLane[38]	ICCV 2021	ResNet34	90.58	78.45	56.48	15.59	52.25	19.6	136.5
CondLane[38]	ICCV 2021	ResNet101	91.54	82.09	65.30	30.68	57.76	44.8	60.2
CLRNet[22]	CVPR 2022	ResNet18	90.96	83.23	68.53	34.78	59.81	11.9	105.0
CLRNet[22]	CVPR 2022	ResNet34	91.56	82.43	65.61	30.20	58.14	21.5	90.0
CLRNet[22]	CVPR 2022	ResNet101	91.58	85.19	73.38	41.02	64.47	42.9	47.7
CLRNet[22]	CVPR 2022	DLA34	92.09	83.98	72.15	41.61	62.28	18.5	81.3
FLAMNet[23]	IEEE TITS 2023	ResNet34	89.94	78.90	55.32	12.96	50.99	30.1	32.0
FLAMNet[23]	IEEE TITS 2023	DLA34	91.16	82.77	64.95	24.22	56.70	21.7	31.7
DBNet[35]	IEEE TIV 2024	ResNet18	89.61	81.27	65.27	26.15	56.52	22.64	147.6
DBNet[35]	IEEE TIV 2024	ResNet34	90.02	83.44	71.66	40.51	60.94	32.1	129.0
Ours	-	SwinGFFM-t	92.34	84.65	70.99	35.77	60.82	12.0	70.4 / 304.7*
Ours	-	SwinGFFM-s	95.04(2.95↑)	88.61(3.42↑)	77.32(3.94↑)	45.02(3.41↑)	65.60(3.13↑)	20.3	38.2 / 192.9*

Note: For a fairer comparison, we re-evaluated the FPS of the source code available detectors using one NVIDIA GeForce RTX 3090 GPU on the same machine. * indicates the FPS after acceleration with TensorRT.

Table 3
Comparison with Advanced Lane Detection on FoggyCULane dataset

Method	Venue	Backbone	Normal	Crowded	Dazzle light	Shadow	No line	Arrow	Curve	Cross	Night	Total
SCNN[14]	AAAI 2018	VGG16	91.07	71.32	67.23	65.23	49.14	88.06	67.07	1344	70.78	72.94
UFLD[15]	ECCV 2020	ResNet18	87.57	65.47	55.21	60.38	38.66	82.26	57.29	1849	60.61	67.69
UFLD[15]	ECCV 2020	ResNet34	89.10	68.29	60.91	62.03	41.98	85.17	63.88	2371	70.13	70.13
LaneATT[21]	CVPR 2020	ResNet18	90.52	71.52	65.70	68.92	47.31	86.32	62.34	870	67.64	74.30
LaneATT[21]	CVPR 2020	ResNet34	91.68	72.93	67.23	65.23	49.14	88.06	67.07	1344	70.78	75.53
LaneATT[21]	CVPR 2020	ResNet122	91.12	74.68	68.87	78.61	47.33	85.76	63.88	1008	69.72	76.16
LSTR[34]	WACV 2021	ResNet34	85.79	63.45	56.73	58.72	38.20	79.31	55.34	1068	57.62	65.64
RESA[32]	AAAI 2021	ResNet34	90.97	72.32	67.31	74.01	46.52	86.32	65.26	1536	73.62	74.97
RESA[32]	AAAI 2021	ResNet50	92.09	73.49	67.40	73.87	47.92	87.48	69.28	1722	69.85	75.19
CondLane[38]	ICCV 2021	ResNet18	91.56	74.41	71.12	77.89	48.59	86.73	71.34	1262	71.00	76.46
CondLane[38]	ICCV 2021	ResNet34	91.76	75.55	69.62	74.62	50.01	87.40	71.29	1427	72.11	77.06
CondLane[38]	ICCV 2021	ResNet101	92.47	76.26	70.91	78.50	51.84	88.93	72.51	1597	72.75	77.90
CLRNet[22]	CVPR 2022	ResNet18	92.55	76.47	71.89	74.45	50.82	88.94	65.93	1122	72.86	78.04
CLRNet[22]	CVPR 2022	ResNet34	92.96	76.32	73.40	79.06	51.46	89.39	71.83	1301	73.64	78.36
CLRNet[22]	CVPR 2022	ResNet101	92.95	76.67	71.49	79.89	52.47	89.29	68.72	1101	73.03	78.72
CLRNet[22]	CVPR 2022	DLA34	93.23	77.64	73.90	79.23	52.11	89.45	72.48	1109	74.63	79.04
FLAMNet[23]	IEEE TITS 2023	ResNet34	92.60	76.61	71.42	79.81	50.89	89.04	71.47	1073	74.17	78.45
FLAMNet[23]	IEEE TITS 2023	DLA34	92.98	77.26	71.84	79.76	51.29	89.34	71.38	1143	73.93	78.77
DBNet[35]	IEEE TIV 2024	ResNet18	84.91	69.27	60.86	67.94	45.69	79.04	67.50	1045	68.57	71.33
DBNet[35]	IEEE TIV 2024	ResNet34	85.61	69.35	61.22	66.50	45.73	79.19	66.51	837	69.93	71.87
Ours	-	SwinGFFM-t	92.68	77.50	71.52	80.42	50.95	88.92	72.08	950	73.11	78.66
Ours	-	SwinGFFM-s	93.40(0.17↑)	78.63(1.99↑)	73.89	82.74(2.85↑)	53.75(1.28↑)	89.82(0.37↑)	74.09(1.58↑)	1146	74.97(0.80↑)	79.85(0.81↑)

Note: Our method attains state-of-the-art (SOTA) results in multiple scenarios including Normal, Crowded, Shadow, No-line, Arrow, Curve and Night conditions, as well as in the overall (Total) performance. Meanwhile, in the Dazzle Light scenario, our method is only 0.01 percentage points behind the leading performance.

5.3. Implementation Details

We conducted our experiments on the NVIDIA GeForce RTX 3090 platform. To achieve better and more stable performance[60], we first pre-trained the SwinGFFM backbone network on the COCO dataset for 500 epochs. Subsequently, during the training process for lane detection tasks, we loaded the pre-trained weights of the backbone network and resized the input images to 800×320 . Additionally, we applied various data augmentation techniques to the input images, including rotation, horizontal flipping, brightness adjustment, and random scaling and cropping. During training, the batch size was set to 16, with an initial learning rate of 3×10^{-4} , using the Adam optimizer and a Step learning rate decay strategy. For detailed network parameters and training settings, please refer to our open-source code.

For objective benchmarking against established lane detection methods including SCNN, RESA, LaneATT, CLRNet, FLAMNet, LSTR, DBNet, UFLD, and CondLane, we replicated these methods on our experimental platform. Given the differences in the architecture of each algorithm, the required batch size, number of training epochs, and learning rate vary, and forcing uniform training settings could negatively impact model performance. Therefore, we adhered to the training configurations provided in the respective papers. Specifically, as the FoggyCULane and FoggyTusimple

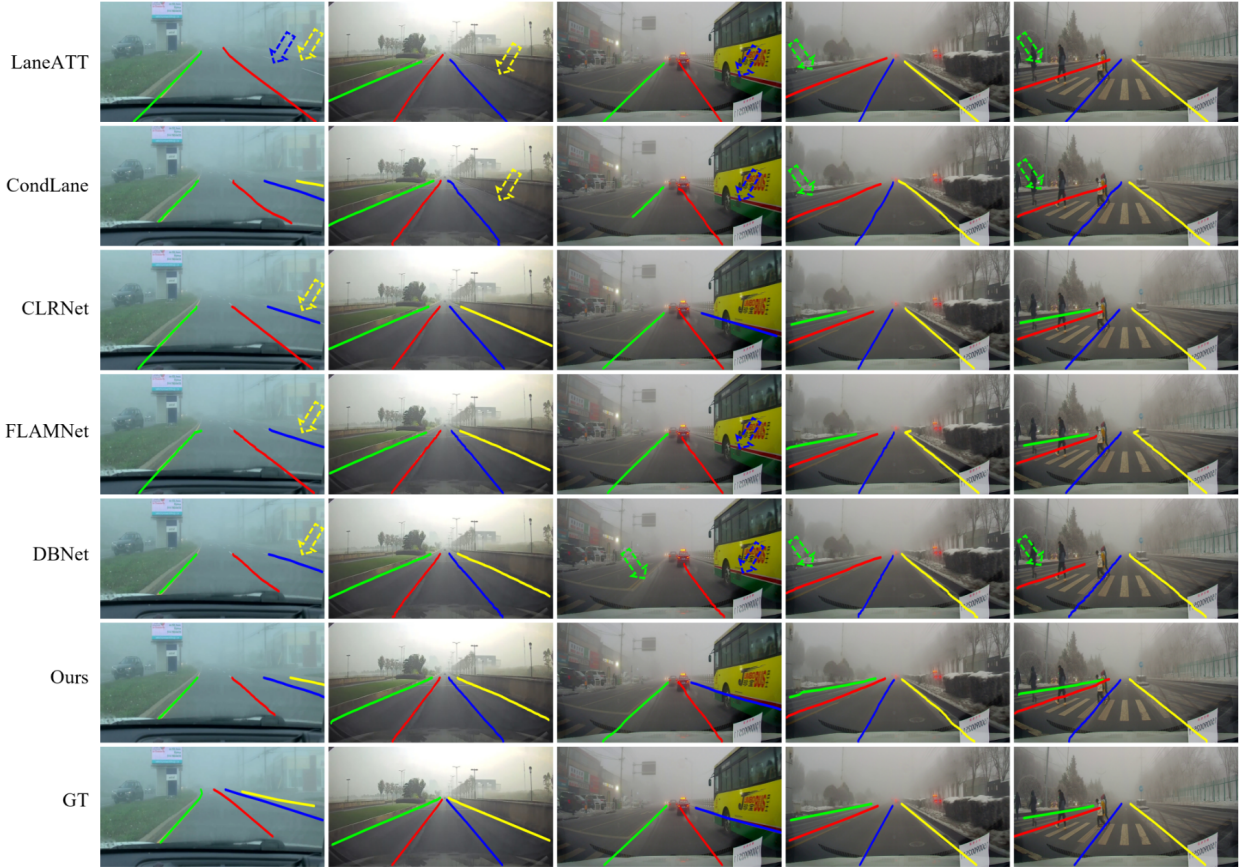


Figure 11: Visualization results of LaneATT, CondLane, CLRNet, FLAMNet, DBNet, and our method on FoggyLane testing set. The arrows indicate instances of lane lines that were not correctly detected by the corresponding method.

datasets are extended versions of the CULane and Tusimple datasets, we adopted the original training parameters from CULane and Tusimple when evaluating the algorithms on FoggyCULane and FoggyTusimple. For the FoggyLane dataset, we used the training parameters from CULane and extended the training epochs to ensure sufficient training, thereby obtaining reliable test results.

5.4. Quantitative Results

5.4.1. Results on FoggyLane

We evaluated our proposed method on the FoggyLane dataset and compared it with other leading lane detection methods. As shown in the Tabel 2, we mainly compared the methods in terms of F1 scores, computational complexity (GFlops), processing speed (FPS).

From the Table 2, it is evident that our method achieves state-of-the-art performance on the foggy lane detection dataset FoggyLane, with F1@50, F1@65, F1@75, and F1@85 scores of 95.04, 88.61, 77.32, and 45.02, respectively. These results surpass the best-performing alternative methods by margins of 2.95%, 3.42%, 3.94%, and 3.41%. The mean F1 (mF1) score demonstrates a 3.13% improvement over the strongest competing approach. Notably, the SwinGFFM-t variant achieves an F1@50 score of 92.34, which even exceeds the performance of DLA34-based CLRNet, previously the top-performing method among comparative approaches.

5.4.2. Results on FoggyCULane

We compared our method with other advanced lane detection methods on the FoggyCULane dataset. As shown in the Table 3, our method consistently achieved the best performance across various scenarios, including Normal, Crowded, shadow, No line, Arrow, Night and Curve. Additionally, our model achieved the highest overall F1 score of 79.81, which achieves a 0.81% improvement over the best alternative method.

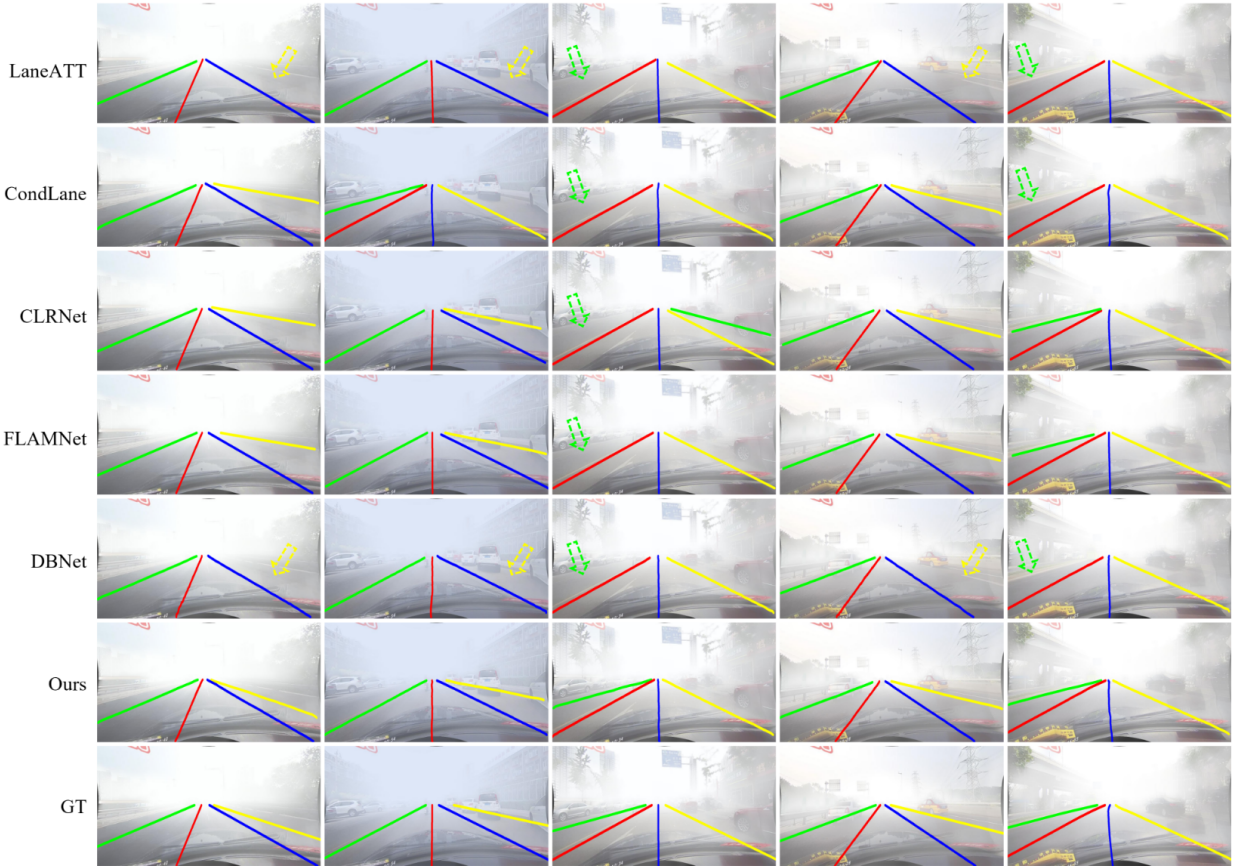


Figure 12: Visualization results of LaneATT, CondLane, CLRNet, FLAMNet, DBNet, and our method on FoggyCULane testing set. The arrows indicate instances of lane lines that were not correctly detected by the corresponding method.

5.4.3. Results on FoggyTusimple

As shown in the Table 4, the traffic scenes in the FoggyTusimple dataset are relatively simple, resulting in smaller performance differences between methods. Nonetheless, our method achieved an F1 score of 96.95, outperforming the best existing method by 0.43%. This further demonstrates the effectiveness of our method in foggy conditions.

5.5. Ablation Study

To explore the effectiveness of each part of the model, we conducted ablation studies on both real and synthetic datasets, namely FoggyLane and FoggyCULane. We have studied the roles of the GFFM, KFFM, and LEEM modules in the model, with Swin-t as the backbone network. As shown in the Tables. 5 and 6, adding each module boosts the model's performance on both datasets. Among them, GFFM contributes the most to the model's improvement, with increases of 1.07 on FoggyLane and 0.41 on FoggyCULane. This indicates that GFFM can effectively capture both local and global information, enriching the feature representation. Building on the foundation of GFFM, the addition of the KFFM module further increases the F1-score by 0.63 on FoggyLane and by 0.26 on FoggyCULane. GFFM is capable of automatically learning the associations between lane instance instances, making full use of relevant information. On this basis, the introduction of the LEEM module enhances the network's focus on edge information. The F1-score increases by 0.28 on FoggyLane and by 0.14 on FoggyCULane.

5.6. Model deployment

After considering the deployment of several edge computing tasks[61, 62], we further evaluate the performance of our algorithm in real-world scenarios. In addition to experiments on existing datasets, we also deployed and tested the model on the vehicle. Specifically, we implemented an edge computing system on the vehicle, as illustrated in the Fig. 14. This system comprises the NVIDIA Jetson AGX Orin edge computing device, a monitor, a camera, and a power

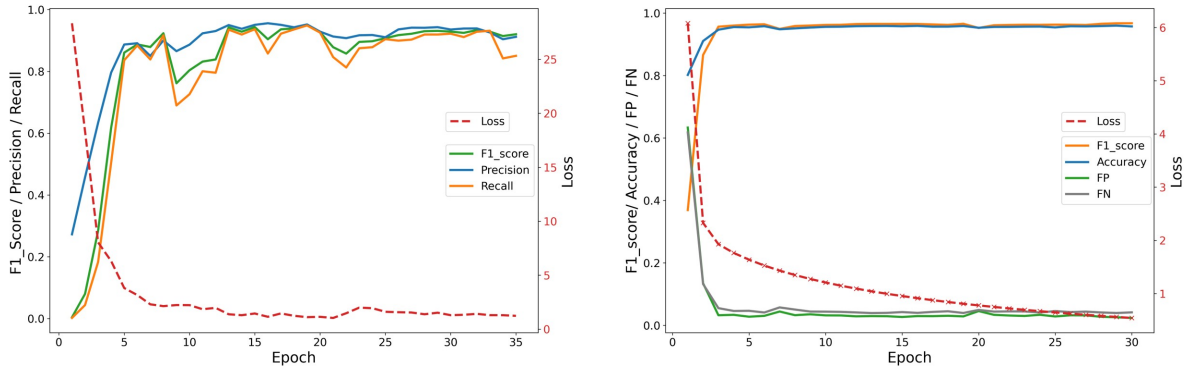


Figure 13: Several metrics of our model's performance during the training process on the FoggyLane and FoggyTusimple datasets, with results on FoggyLane on the left and FoggyTusimple on the right.

Table 4

Comparison with Advanced Lane Detection on FoggyTusimple dataset.

Method	Venue	Backbone	F1(%)	ACC(%)	FP(%)	FN(%)
SCNN[14]	AAAI 2018	VGG16	94.64	95.89	5.87	4.78
UFLD[15]	ECCV 2020	ResNet18	94.57	93.60	3.49	7.59
UFLD[15]	ECCV 2020	ResNet34	95.05	95.10	4.84	5.08
LaneATT[21]	CVPR 2020	ResNet18	95.77	95.78	3.83	3.53
LaneATT[21]	CVPR 2020	ResNet34	96.15	95.50	4.59	3.06
LaneATT[21]	CVPR 2020	ResNet122	93.24	95.43	9.61	3.50
LSTR[34]	WACV 2021	ResNet34	94.70	95.58	5.74	4.81
RESA[32]	AAAI 2021	ResNet34	95.22	95.60	4.63	4.95
RESA[32]	AAAI 2021	ResNet50	95.51	95.83	4.53	4.43
CondLane[38]	ICCV 2021	ResNet18	95.41	94.81	3.80	5.46
CondLane[38]	ICCV 2021	ResNet34	95.65	94.69	3.63	5.13
CondLane[38]	ICCV 2021	ResNet101	96.03	95.14	2.94	5.09
CLRNet[22]	CVPR 2022	ResNet18	96.48	95.64	3.89	3.11
CLRNet[22]	CVPR 2022	ResNet34	96.23	95.94	4.34	3.17
CLRNet[22]	CVPR 2022	ResNet101	96.13	95.64	4.15	3.58
FLAMNet[23]	IEEE TITS 2023	ResNet18	96.52	95.65	3.84	3.09
FLAMNet[23]	IEEE TITS 2023	ResNet101	96.34	95.98	4.45	2.82
DBNet[35]	IEEE TIV 2024	ResNet18	95.71	93.89	3.53	5.12
DBNet[35]	IEEE TIV 2024	ResNet34	95.61	93.72	3.48	5.38
Ours	-	SwinGFFM-t	96.63	95.86	2.77	4.04
Ours	-	SwinGFFM-s	96.95(0.43↑)	96.10(0.12↑)	2.32(0.62↓)	3.83

supply unit. The results of the evaluation demonstrate that our approach can operate in real-time with high accuracy on the vehicle's edge computing platform, despite the constraints on computational resources.

6. Conclusion

This study focuses on lane detection in foggy conditions, aiming to address the range of challenges posed by foggy environments, which is crucial for ensuring driving safety in fog and enhancing Advanced Driver Assistance System (ADAS) capabilities. To address the current lack of publicly available datasets for lane detection in foggy conditions, we constructed a real-world foggy lane dataset, FoggyLane, and synthesized two additional foggy datasets, FoggyCULane and FoggyTusimple, based on the popular CULane and Tusimple datasets.

In response to the challenges of lane detection in foggy scenarios, we propose an end-to-end fog-enhanced lane detection method. First, this method incorporates a Global Feature Fusion Module in the backbone network to address the absence of global spatial information in foggy scenes. Second, we employ a dynamic convolution-based detection

Table 5

Ablation experiments of different components on the FoggyLane dataset.

Model	GFFM	KFFM	LEEM	F1-score	Gflops(G)
Baseline				90.36	13.77
	✓			91.43	11.94
	✓	✓		92.06	11.97
Ours	✓	✓	✓	92.34↑	12.01

Table 6

Ablation experiments of different components on the FoggyCULane dataset.

Model	GFFM	KFFM	LEEM	F1-score	Gflops(G)
Baseline				77.85	13.77
	✓			78.26	11.94
	✓	✓		78.52	11.97
Ours	✓	✓	✓	78.66↑	12.01



Figure 14: A edge computing system built with NVIDIA Jetson AGX Orin. After experimental validation, it has been demonstrated that our method can run accurately on the vehicle's edge computing platform with limited computational resources, achieving a performance of 38.4 FPS.

head for instance-sensitive lane segmentation, integrating a Kernel Feature Fusion Module within the detection head to automatically capture associations between lane instances. Additionally, a Low-Level Edge Enhancement Module was added to increase the network's focus on edge information, mitigating the loss of edge details and improving lane detection accuracy under foggy conditions.

Comparative experiments on the FoggyLane, FoggyCULane, and FoggyTusimple datasets with other advanced lane detection methods demonstrate that our approach achieves superior performance in both clear and foggy conditions, significantly improving lane detection accuracy. Furthermore, with TensorRT acceleration, our method achieves an inference speed of 38.4 FPS on the NVIDIA Jetson AGX Orin, further validating its practical applicability in real-world scenarios.

Acknowledgments

This project is jointly supported by National Natural Science Foundation of China (Nos. 52172350, W2421069 and 51775565), the Guangdong Basic and Applied Research Foundation (No. 2022B1515120072), the Guangzhou Science and Technology Plan Project (No. 2024B01W0079), the Nansha Key RD Program (No. 2022ZD014), the Science and

Technology Planning Project of Guangdong Province (No. 2023B1212060029). [We would like to release our source code and dataset.](#)

Compliance with ethics guidelines

Ronghui Zhang, Yuhang Ma, Tengfei Li, Ziyu Lin, Yueying Wu, Junzhou Chen, Lin Zhang, Jia Hu, Tony Z. Qiu and Konghui Guo declare that they have no conflict of interest or financial conflicts to disclose.

References

- [1] C. Li, W. Liu, H. Yang, Deep causal inference for understanding the impact of meteorological variations on traffic, *Transportation Research Part C: Emerging Technologies* 165 (2024) 104744. doi:<https://doi.org/10.1016/j.trc.2024.104744>.
- [2] H. Guo, M. Keyvan-Ekbatani, K. Xie, Lane change detection and prediction using real-world connected vehicle data, *Transportation Research Part C: Emerging Technologies* 142 (2022) 103785. doi:<https://doi.org/10.1016/j.trc.2022.103785>.
- [3] Y. Xing, Y. Wu, H. Wang, L. Wang, L. Li, Y. Peng, Failed lane-changing detection and prediction using naturalistic vehicle trajectories, *Transportation Research Part C: Emerging Technologies* 170 (2025) 104939. doi:<https://doi.org/10.1016/j.trc.2024.104939>.
- [4] K. Grosse, A. Alahi, A qualitative ai security risk assessment of autonomous vehicles, *Transportation Research Part C: Emerging Technologies* 169 (2024) 104797. doi:<https://doi.org/10.1016/j.trc.2024.104797>.
- [5] Pexels, <https://www.pexels.com/zh-cn/>, 2025.
- [6] J. Son, H. Yoo, S. Kim, K. Sohn, Real-time illumination invariant lane detection for lane departure warning system, *Expert Systems with Applications* 42 (2015) 1816–1824. doi:<https://doi.org/10.1016/j.eswa.2014.10.024>.
- [7] C. Hou, J. Hou, C. Yu, An efficient lane markings detection and tracking method based on vanishing point constraints, in: *Chinese Control Conference (CCC)*, IEEE, 2016, pp. 6999–7004. doi:10.1109/ChiCC.2016.7554460.
- [8] W. Wang, W. Zhang, Crrfnet: An adaptive traffic object detection method based on camera and radar radio frequency fusion, *Transportation Research Part C: Emerging Technologies* 166 (2024) 104791. doi:<https://doi.org/10.1016/j.trc.2024.104791>.
- [9] D. Yang, Y. Wu, F. Sun, J. Chen, D. Zhai, C. Fu, Freeway accident detection and classification based on the multi-vehicle trajectory data and deep learning model, *Transportation Research Part C: Emerging Technologies* 130 (2021) 103303. doi:<https://doi.org/10.1016/j.trc.2021.103303>.
- [10] Y. Qi, C. Liu, M. Scaioni, Y. Li, Y. Qiao, X. Ma, H. Wu, K. Zhang, D. Wang, Geometric information constraint 3d object detection from lidar point cloud for autonomous vehicles under adverse weather, *Transportation Research Part C: Emerging Technologies* 161 (2024) 104555. doi:<https://doi.org/10.1016/j.trc.2024.104555>.
- [11] D. Neven, B. De Brabandere, S. Georgoulis, M. Proesmans, L. Van Gool, Towards end-to-end lane detection: an instance segmentation approach, in: *2018 IEEE Intelligent Vehicles Symposium (IV)*, IEEE, 2018, pp. 286–291. doi:10.1109/IVS.2018.8500547.
- [12] H. Abualsaud, S. Liu, D. B. Lu, K. Situ, A. Rangesh, M. M. Trivedi, Laneaf: Robust multi-lane detection with affinity fields, *IEEE Robotics and Automation Letters* 6 (2021) 7477–7484. doi:10.1109/LRA.2021.3098066.
- [13] F. Yu, D. Wang, E. Shelhamer, T. Darrell, Deep layer aggregation, in: *Proceedings of the IEEE Conference on Computer Vision and Pattern Recognition*, 2018, pp. 2403–2412. doi:10.1109/CVPR.2018.00255.
- [14] X. Pan, J. Shi, P. Luo, X. Wang, X. Tang, Spatial as deep: Spatial cnn for traffic scene understanding, in: *Proceedings of the AAAI Conference on Artificial Intelligence*, volume 32, 2018.
- [15] Z. Qin, H. Wang, X. Li, Ultra fast structure-aware deep lane detection, in: *European Conference on Computer Vision*, Springer, 2020, pp. 276–291. doi:10.1007/978-3-030-58586-0_17.
- [16] J. Redmon, You only look once: Unified, real-time object detection, in: *Proceedings of the IEEE Conference on Computer Vision and Pattern Recognition*, 2016, pp. 779–788. doi:10.1109/CVPR.2016.91.
- [17] A. Farhadi, J. Redmon, Yolov3: An incremental improvement, *arXiv preprint arXiv:1804.02767* (2018) 1–6. doi:10.48550/arXiv.1804.02767.
- [18] S. Ren, K. He, R. Girshick, J. Sun, Faster r-cnn: Towards real-time object detection with region proposal networks, *IEEE Transactions on Pattern Analysis and Machine Intelligence* 39 (2016) 1137–1149. doi:10.1109/TPAMI.2016.2577031.
- [19] W. Liu, D. Anguelov, D. Erhan, C. Szegedy, S. Reed, C.-Y. Fu, A. C. Berg, Ssd: Single shot multibox detector, in: *European Conference on Computer Vision*, Springer, 2016, pp. 21–37. doi:10.1007/978-3-319-46448-0_2.
- [20] Z. Chen, Q. Liu, C. Lian, Pointlanenet: Efficient end-to-end cnns for accurate real-time lane detection, in: *2019 IEEE Intelligent Vehicles Symposium (IV)*, IEEE, 2019, pp. 2563–2568. doi:10.1109/IVS.2019.8813778.
- [21] L. Tabelini, R. Berriel, T. M. Paixao, C. Badue, A. F. De Souza, T. Oliveira-Santos, Keep your eyes on the lane: Real-time attention-guided lane detection, in: *Proceedings of the IEEE/CVF Conference on Computer Vision and Pattern Recognition*, 2021, pp. 294–302. doi:10.1109/CVPR46437.2021.00036.
- [22] T. Zheng, Y. Huang, Y. Liu, W. Tang, Z. Yang, D. Cai, X. He, Clrnet: Cross layer refinement network for lane detection, in: *Proceedings of the IEEE/CVF Conference on Computer Vision and Pattern Recognition*, 2022, pp. 898–907. doi:10.1109/CVPR52688.2022.00097.
- [23] H. Ran, Y. Yin, F. Huang, X. Bao, Flamnet: A flexible line anchor mechanism network for lane detection, *IEEE Transactions on Intelligent Transportation Systems* 24 (2023) 12767–12778. doi:10.1109/TITS.2023.3290991.
- [24] W. Zhao, C. Roncoli, A constrained spectral clustering method for lane identification using trajectory data, *Transportation Research Part C: Emerging Technologies* 155 (2023) 104270. doi:<https://doi.org/10.1016/j.trc.2023.104270>.
- [25] S.-C. Huang, T.-H. Le, D.-W. Jaw, Dsnet: Joint semantic learning for object detection in inclement weather conditions, *IEEE Transactions on Pattern Analysis and Machine Intelligence* 43 (2020) 2623–2633. doi:10.1109/TPAMI.2020.2977911.

- [26] X. Nie, Z. Xu, W. Zhang, X. Dong, N. Liu, Y. Chen, Foggy lane dataset synthesized from monocular images for lane detection algorithms, *Sensors* 22 (2022) 5210. doi:10.3390/s22145210.
- [27] Y. Chen, W. Li, C. Sakaridis, D. Dai, L. Van Gool, Domain adaptive faster r-cnn for object detection in the wild, in: *Proceedings of the IEEE Conference on Computer Vision and Pattern Recognition*, 2018, pp. 3339–3348. doi:10.1109/CVPR.2018.00352.
- [28] S. Zhang, H. Tuo, J. Hu, Z. Jing, Domain adaptive yolo for one-stage cross-domain detection, in: *Asian Conference on Machine Learning*, PMLR, 2021, pp. 785–797.
- [29] M. Hnewa, H. Radha, Multiscale domain adaptive yolo for cross-domain object detection, in: *Proceedings of the IEEE International Conference on Image Processing*, 2021, pp. 3323–3327. doi:10.1109/ICIP42928.2021.9506039.
- [30] J. Li, R. Xu, J. Ma, Q. Zou, J. Ma, H. Yu, Domain adaptive object detection for autonomous driving under foggy weather, in: *Proceedings of the IEEE/CVF Winter Conference on Applications of Computer Vision*, 2023, pp. 612–622.
- [31] Tusimple, <https://github.com/TuSimple/tusimple-benchmark>, 2017.
- [32] T. Zheng, H. Fang, Y. Zhang, W. Tang, Z. Yang, H. Liu, D. Cai, Resa: Recurrent feature-shift aggregator for lane detection, in: *Proceedings of the AAAI Conference on Artificial Intelligence*, volume 35, 2021, pp. 3547–3554. doi:10.1609/aaai.v35i4.16469.
- [33] L. Tabelini, R. Berriel, T. M. Paixao, C. Badue, A. F. De Souza, T. Oliveira-Santos, PolyLaneNet: Lane estimation via deep polynomial regression, in: *Proceedings of the IEEE International Conference on Pattern Recognition*, IEEE, 2021, pp. 6150–6156. doi:10.1109/ICPR48806.2021.9412265.
- [34] R. Liu, Z. Yuan, T. Liu, Z. Xiong, End-to-end lane shape prediction with transformers, in: *Proceedings of the IEEE/CVF Winter Conference on Applications of Computer Vision*, 2021, pp. 3694–3702. doi:10.1109/WACV48630.2021.00374.
- [35] X. Dai, J. Xie, G. Zhang, K. Chang, F. Chen, Z. Wang, C. Tang, Dbnet: A curve-based dynamic association framework for lane detection, *IEEE Transactions on Intelligent Vehicles* (2024). doi:10.1109/TIV.2024.3370213.
- [36] X. Li, J. Li, X. Hu, J. Yang, Line-cnn: End-to-end traffic line detection with line proposal unit, *IEEE Transactions on Intelligent Transportation Systems* 21 (2019) 248–258. doi:10.1109/TITS.2019.2890870.
- [37] S. Yoo, H. S. Lee, H. Myeong, S. Yun, H. Park, J. Cho, D. H. Kim, End-to-end lane marker detection via row-wise classification, in: *Proceedings of the IEEE/CVF Conference on Computer Vision and Pattern Recognition Workshops*, 2020, pp. 1006–1007. doi:10.1109/CVPRW50498.2020.00511.
- [38] L. Liu, X. Chen, S. Zhu, P. Tan, CondlaneNet: a top-to-down lane detection framework based on conditional convolution, in: *Proceedings of the IEEE/CVF International Conference on Computer Vision*, 2021, pp. 3773–3782. doi:10.1109/ICCV48922.2021.00375.
- [39] GoogleMaps, <https://www.google.com/maps>, Accessed: 2024.
- [40] K. Behrendt, R. Soussan, Unsupervised labeled lane markers using maps, in: *Proceedings of the IEEE/CVF International Conference on Computer Vision Workshops*, 2019, pp. 832–839. doi:10.1109/ICCVW.2019.00111.
- [41] YouTube, <https://www.youtube.com/>, Accessed: 2024.
- [42] M. Aly, Real time detection of lane markers in urban streets, in: *2008 IEEE Intelligent Vehicles Symposium (IV)*, IEEE, 2008, pp. 7–12. doi:10.1109/IVS.2008.4621152.
- [43] X. Huang, X. Cheng, Q. Geng, B. Cao, D. Zhou, P. Wang, Y. Lin, R. Yang, The apolloScape dataset for autonomous driving, in: *Proceedings of the IEEE Conference on Computer Vision and Pattern Recognition Workshops*, 2018, pp. 954–960. doi:10.1109/CVPRW.2018.00141.
- [44] F. Yu, H. Chen, X. Wang, W. Xian, Y. Chen, F. Liu, V. Madhavan, T. Darrell, Bdd100k: A diverse driving dataset for heterogeneous multitask learning, in: *Proceedings of the IEEE/CVF Conference on Computer Vision and Pattern Recognition*, 2020, pp. 2636–2645. doi:10.1109/CVPR42600.2020.00271.
- [45] H. Xu, S. Wang, X. Cai, W. Zhang, X. Liang, Z. Li, Curvelane-nas: Unifying lane-sensitive architecture search and adaptive point blending, in: *European Conference on Computer Vision*, Springer, 2020, pp. 689–704. doi:10.1007/978-3-030-58555-6_41.
- [46] R. Zhang, J. Peng, W. Gou, Y. Ma, J. Chen, H. Hu, W. Li, G. Yin, Z. Li, A robust and real-time lane detection method in low-light scenarios to advanced driver assistance systems, *Expert Systems with Applications* 256 (2024) 124923. doi:10.1016/j.eswa.2024.124923.
- [47] K. Harald, Theorie der horizontalen sichtweite: Kontrast und sichtweite, Keim and Nemnich, Munich 12 (1924) 33–53. doi:10.1007/978-3-663-04661-5_2.
- [48] X. Chen, Y. Wang, X. Chen, W. Zeng, S2r-depthnet: Learning a generalizable depth-specific structural representation, in: *Proceedings of the IEEE/CVF Conference on Computer Vision and Pattern Recognition*, 2021, pp. 3034–3043. doi:10.1109/CVPR46437.2021.00305.
- [49] K. He, J. Sun, X. Tang, Single image haze removal using dark channel prior, *IEEE Transactions on Pattern Analysis and Machine Intelligence* 33 (2011) 2341–2353. doi:10.1109/TPAMI.2010.168.
- [50] J. Wang, K. Sun, T. Cheng, B. Jiang, C. Deng, Y. Zhao, D. Liu, Y. Mu, M. Tan, X. Wang, W. Liu, B. Xiao, Deep high-resolution representation learning for visual recognition, *IEEE Transactions on Pattern Analysis and Machine Intelligence* 43 (2021) 3349–3364. doi:10.1109/TPAMI.2020.2983686.
- [51] R. Zhang, S. Yang, D. Lyu, Z. Wang, J. Chen, Y. Ren, B. Gao, Z. Lv, Agsnet: A robust road ponding detection method for proactive traffic safety, *IEEE Transactions on Intelligent Transportation Systems* 26 (2025) 497–516. doi:10.1109/TITS.2024.3506659.
- [52] J. Chen, N. Zhao, R. Zhang, L. Chen, K. Huang, Z. Qiu, Refined crack detection via lecsformer for autonomous road inspection vehicles, *IEEE Transactions on Intelligent Vehicles* 8 (2023) 2049–2061. doi:10.1109/TIV.2022.3204583.
- [53] R. Zhang, J. Peng, W. Gou, Y. Ma, J. Chen, H. Hu, W. Li, G. Yin, Z. Li, A robust and real-time lane detection method in low-light scenarios to advanced driver assistance systems, *Expert Systems with Applications* 256 (2024) 124923. doi:10.1016/j.eswa.2024.124923.
- [54] Z. Liu, Y. Lin, Y. Cao, H. Hu, Y. Wei, Z. Zhang, S. Lin, B. Guo, Swin transformer: Hierarchical vision transformer using shifted windows, in: *Proceedings of the IEEE/CVF International Conference on Computer Vision*, 2021, pp. 10012–10022. doi:10.1109/ICCV48922.2021.00986.
- [55] Z. Liu, H. Hu, Y. Lin, Z. Yao, Z. Xie, Y. Wei, J. Ning, Y. Cao, Z. Zhang, L. Dong, et al., Swin transformer v2: Scaling up capacity and resolution, in: *Proceedings of the IEEE/CVF Conference on Computer Vision and Pattern Recognition*, 2022, pp. 12009–12019. doi:10.1109/CVPR52688.2022.01170.

- [56] X. Dong, J. Bao, D. Chen, W. Zhang, N. Yu, L. Yuan, D. Chen, B. Guo, Cswin transformer: A general vision transformer backbone with cross-shaped windows, in: Proceedings of the IEEE/CVF Conference on Computer Vision and Pattern Recognition, 2022, pp. 12124–12134. doi:10.1109/CVPR52688.2022.01181.
- [57] Z. Tian, B. Zhang, H. Chen, C. Shen, Instance and panoptic segmentation using conditional convolutions, IEEE Transactions on Pattern Analysis and Machine Intelligence 45 (2023) 669–680. doi:10.1109/TPAMI.2022.3145407.
- [58] X. Wang, T. Kong, C. Shen, Y. Jiang, L. Li, Solo: Segmenting objects by locations, in: European Conference on Computer Vision, Springer, 2020, pp. 649–665. doi:doi.org/10.1007/978-3-030-58523-5_38.
- [59] X. Wang, R. Zhang, T. Kong, L. Li, C. Shen, Solov2: Dynamic and fast instance segmentation, Advances in Neural Information Processing Systems 33 (2020) 17721–17732.
- [60] I. Amos, J. Berant, A. Gupta, Never train from scratch: Fair comparison of long-sequence models requires data-driven priors, in: Proceedings of the International Conference on Learning Representations, 2024, pp. 1–14.
- [61] H. F. Yang, Y. Ling, C. Kopca, S. Ricord, Y. Wang, Cooperative traffic signal assistance system for non-motorized users and disabilities empowered by computer vision and edge artificial intelligence, Transportation Research Part C: Emerging Technologies 145 (2022) 103896. doi:https://doi.org/10.1016/j.trc.2022.103896.
- [62] H. F. Yang, J. Cai, C. Liu, R. Ke, Y. Wang, Cooperative multi-camera vehicle tracking and traffic surveillance with edge artificial intelligence and representation learning, Transportation Research Part C: Emerging Technologies 148 (2023) 103982. doi:https://doi.org/10.1016/j.trc.2022.103982.